Gold Nanoshell Nanomicelles for Potential Magnetic Resonance Imaging, Light-Triggered Drug Release, and Photothermal Therapy

*Yan Ma, Xiaolong Liang, Sheng Tong, Gang Bao, Qiushi Ren, and Zhifei Dai**

A novel multifunctional drug-delivery platform is developed based on cholesteryl succinyl silane (CSS) nanomicelles loaded with doxorubicin, Fe_3O_4 magnetic nanoparticles, and gold nanoshells (CDF-Au-shell nanomicelles) to combine magnetic resonance (MR) imaging, magnetic-targeted drug delivery, light-triggered drug release, and photothermal therapy. The nanomicelles show improved drug-encapsulation efficiency and loading level, and a good response to magnetic fields, even after the formation of the gold nanoshell. An enhancement for T_2-weighted MR imaging is observed for the CDF-Au-shell nanomicelles. These nanomicelles display surface plasmon absorbance in the near-infrared (NIR) region, thus exhibiting an NIR (808 nm)-induced temperature elevation and an NIR light-triggered and stepwise release behavior of doxorubicin due to the unique characteristics of the CSS nanomicelles. Photothermal cytotoxicity in vitro confirms that the CDF-Au-shell nanomicelles cause cell death through photothermal effects only under NIR laser irradiation. Cancer cells incubated with CDF-Au-shell nanomicelles show a significant decrease in cell viability only in the presence of both NIR irradiation and a magnetic field, which is attributed to the synergetic effects of the magnetic-field-guided drug delivery and the photothermal therapy. Therefore, such multicomponent nanomicelles can be developed as a smart and promising nanosystem that integrates multiple capabilities for effective cancer diagnosis and therapy.

1. Introduction

The dose of a drug required to achieve clinically effective cytotoxicity in tumors often causes severe damage to actively propagating non-malignant cells, creating undesirable side effects. To overcome these problems, various drug-delivery strategies with lower systemic toxicity and better drug cell internalization compared with free drug have been studied.[1] Nevertheless, the spatial and temporal control of local drug release is often difficult to achieve in many clinical applications. Light-triggered drug release is an attractive approach for the spatiotemporal control of drug delivery, which may allow for precise, on-demand drug delivery within individual cells in vitro or may enable precise treatment of cancer in vivo. Gold nanoshells mediate a strong surface heat flux upon absorption of NIR light; thus, they are an excellent candidate for NIR light-triggered release of a drug from nanocarriers, as well as a photothermal-treatment agent.[2,3]

When combined with gold nanoshells, liposomes of certain compositions have been shown to be capable of thermally controlled release of encapsulated agents. Their permeability is greatly enhanced around the membrane melting temperature (T_m), which depends on the lipid composition.[4] A drug can thus be released if the liposome membrane is heated above T_m. Using double long-strand alkane-based liposomes as thermoresponsive drug-delivery vehicles, T_m is typically close to body temperature, which results in drug leakage during circulation in the human system. If T_m instead is chosen far above body temperature, leakage during circulation will be much more minimized.[5] On the other hand, due to the insufficient stability of traditional liposomes, the majority of gold-nanoshell-coated liposomes would go through a melting and fusion process, thus forming large gold aggregates so the content in liposomes usually exhibits a one-time release profile instead of multiple release kinetics.[6]

Magnetic-resonance (MR) imaging has become a prominent non-invasive technique in diagnostic clinical medicine owning

Dr. Y. Ma, Prof. Z. Dai
Nanomedicine and Biosensor Laboratory
School of Life Science and Technology
Harbin Institute of Technology
Harbin, 150080, China
E-mail: zhifei.dai@pku.edu.cn
Dr. X. Liang, Prof. Q. Ren, Prof. Z. Dai
Department of Biomedical Engneering
College of Engineering
Peking University
Beijing 100871, China
Dr. S. Tong, Prof. G. Bao
Department of Biomedical Engineering
Georgia Institute of Technology
and Emory University
Atlanta, GA 30332, USA

DOI: 10.1002/adfm.201201663

to the possibility of obtaining highly resolved 3D images of living bodies.[7] Super-paramagnetic iron oxide nanoparticles (SPIO NPs) have received great attention since their development as a T_2 contrast agent. This is the first nanoparticulate MR imaging contrast agent and is still used clinically.[8] SPIO NPs, which can be manipulated and controlled by an external magnetic field, are also sophisticatedly employed in magnetically targeted drug-delivery systems for regulating drug release, minimizing side effects, and improving therapeutic efficacy.[9] Incorporation of iron oxide NPs into liposome membranes is related to their size. Theoretical studies suggest a threshold maximum NP diameter of 6.5 nm for incorporation of NPs into lipid bilayers. Larger NPs preferentially form micelles rather than liposome-like structures.[10] Thus, the volume proportion of hydrophobic space is greatly enhanced and the encapsulation efficiency for hydrophobic nanoparticles and drug are obviously improved. Nevertheless, nanomicelles formed by traditional phospholipids have not attained their full potential as drug-delivery carriers due to their insufficient morphological stability.[11]

Recently, we reported a nanohybrid vesicle with a cholesteryl bilayer structure and an atomic layer of an inorganic polyorganosiloxane network on its surface, fabricated from cholesteryl-succinyl silane (CSS) molecules.[12] Herein, we report the design of gold-nanoshell-coated CSS nanomicelles loaded with both doxorubicin and Fe_3O_4 magnetic nanoparticles (CDF-Au-shell nanomicelles) to combine MR imaging, magnetic-field-guided drug delivery, light-triggered drug release, and photothermal therapy (**Scheme 1**). SPIO NPs loaded in nanomicelles have both MR imaging and magnetic-targeting functions. Gold nanoshells on the outer layer of nanomicelles operate as NIR-light-absorbing agents, which can thus result in effective NIR-triggered release of a drug and photothermal therapy. Compared with conventional systems, such as liposomes, CDF-Au-shell nanomicelles would have more advantages for potential clinical applications: 1) minimization of drug leakage during circulation process in vivo, because the cholesteryl molecule as the hydrophobic part has a melting temperature as high as 150 °C; 2) realization of multiple release kinetics rather than a one-time release profile because the siloxane surface can endow CSS nanomicelles with remarkably high mechanical stability and heat resistance;[12,13] 3) improvement of drug encapsulation efficiency and loading level due to the full hydrophobic interior of CSS nanomicelles; 4) identification of the location and size of tumors, monitoring the therapeutic effectiveness and addressing the drug amount accumulated in the tumor through contrast-enhanced MR imaging; 5) a significant increase of the likelihood of cell killing, greatly improving the selectivity and potentially overcoming resistance to chemotherapeutic agents by the combined MR imaging, photothermal therapy, chemotherapy, and magnetic-field-guided drug delivery. In a word, this new multifunctional platform combines all these functions within a single nanomicelle and yields a substantial promise for highly efficient anticancer treatment.

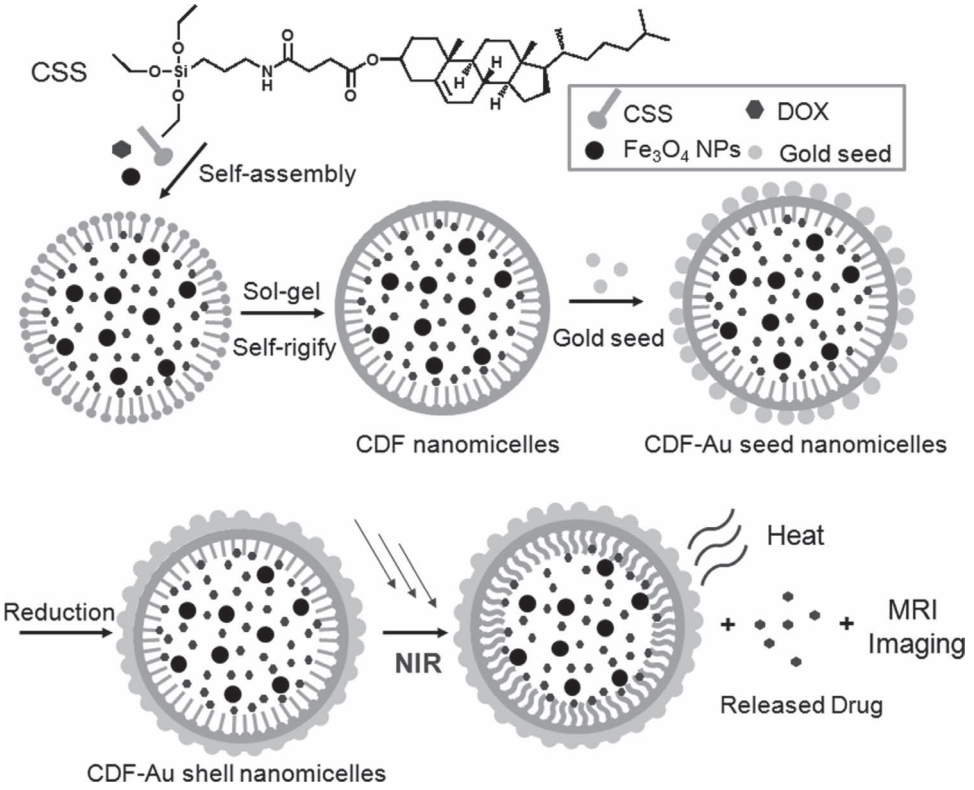

Scheme 1. Schematic illustration of multifunctional CSS nanomicelles that comprise three functional parts, as potential applications in cancer therapy: i) DOX, as a chemotherapeutic agent, ii) Fe_3O_4 nanoparticles for both MR imaging and magnetic-targeted drug delivery, and iii) a gold nanoshell used for both NIR light-triggered drug release and photothermal therapy. Such a nanosystem integrates capabilities for MR imaging and the treatment of cancer. C, D, F, and Au represent the CSS nanomicelles, DOX, the Fe_3O_4 nanoparticles, and the gold, respectively.

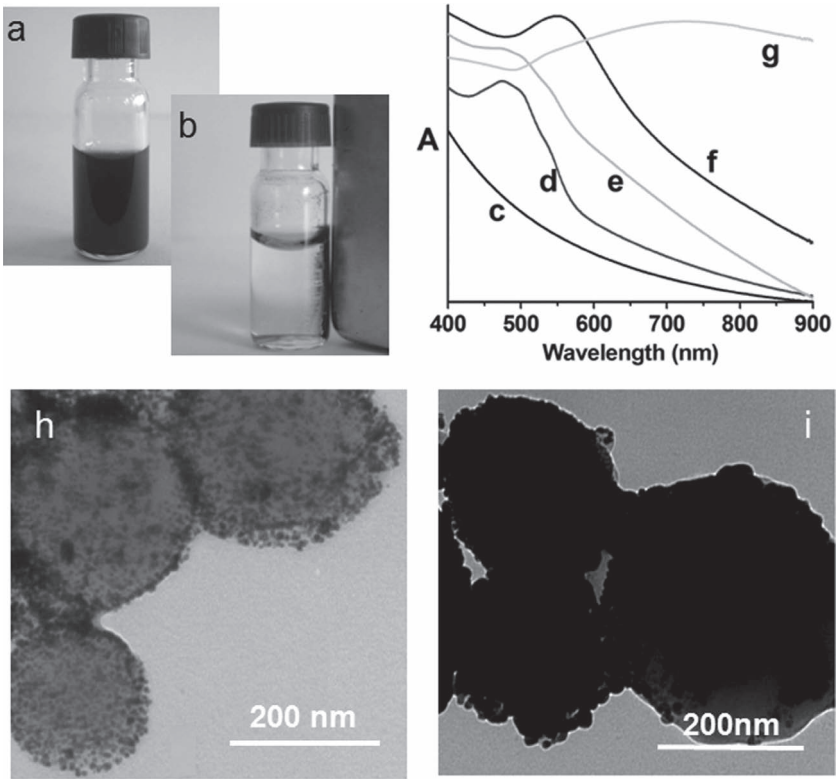

Figure 1. a,b) Response of CDF-Au-shell nanomicelles to a magnetic field. c–g) Absorption spectra of blank CSS vesicles (c), DOX-loaded CSS vesicles (d), CDF nanomicelles (e), CDF-Au-seed nanomicelles (f), and CDF-Au-shell nanomicelles (g). h,i) TEM images of CDF-Au-seed nanomicelles (h) and CDF-Au-shell nanomicelles (i).

2. Results and Discussion

2.1. Preparation and Characterization of Gold-Shell-Coated Nanomicelles

The synthesis of the doxorubicin (DOX)-loaded magnetic nanomicelles (CDF) was a multistep procedure. Firstly, DOX•HCl was converted to its hydrophobic base form by addition of triethylamine, as reported in the literature.[14] Oleic acid-stabilized Fe_3O_4 nanoparticles were synthesized by a coprecipitation method.[15] The average diameter of the Fe_3O_4 NPs was determined to be 8.35 ± 0.74 nm by dynamic light scattering (DLS) measurements. Then, the CDF nanomicelles were prepared by an injection method. In our previous study,[8] CSS is a suitable molecule for forming a liposome-like structure after hydrolyzing the triethoxysilyl group, and oleic acid-stabilized Fe_3O_4 NPs are expected to be loaded into the hydrophobic part of the liposomes. When the diameter of the Fe_3O_4 NPs is larger than 6.5 nm, micelles loaded with Fe_3O_4 NPs will be formed instead of liposomes, according to the literature.[10] Upon ultrasonication, CSS molecules together with DOX and Fe_3O_4 NPs, form nanomicelles via the strong hydrophobic interaction between cholesteryl groups, hydrophobic DOX, and oleic acid-stabilized Fe_3O_4 NPs. Then, the CDF nanomicelles self-rigidify via in situ sol-gel processes on the surface, as reported in our previous study.[13] The resulting siloxane surface adds a remarkably high morphological stability compared with conventional lipid micelles. The size of the CDF nanomicelles was determined to be 272.3 ± 5.5 nm (Supporting Information, Figure S1) and the typical structure of the particles was confirmed by transmission electron microscopy (TEM) (Supporting Information, Figure S1, inset). It could be clearly seen that Fe_3O_4 NPs existed as darker dots in the CDF nanomicelles.

Such CDF nanomicelles are suitable carriers for hydrophobic drugs because of their increased volume proportion of hydrophobic space. When the molar ratio of DOX to CSS molecules was 1:30, the drug encapsulation efficiency (EE) was evaluated to be 92% and the loading level (LL) was 5% as compared with a 53% EE and 2% LL when the oleic acid-stabilized Fe_3O_4 NPs were not added. We also prepared hydrophilic Fe_3O_4 NPs (at the same size range) and DOX-loaded CSS NPs. In this case, vesicles would be formed, but only 34% EE and 1% LL were obtained with similar procedures. Thus, the volume proportion of hydrophobic space was greatly enhanced and the encapsulation efficiency for the hydrophobic nanoparticles and the drug was obviously improved because the CSS formed nanomicelles instead of liposome-like nanoparticles.

Due to the loading of DOX, the surface charge of CDF nanomicelles was evaluated to be about 23.8 ± 2.2 mV after the self-rigidifiication process. Hence, negatively charged gold seeds with a diameter of about 2–3 nm were able to adsorb onto the surface of CDF nanomicelles via electrostatic interactions. Then, a zeta potential of around −13.8 ± 1.4 mV was measured, indicating the successful deposition of gold seeds onto the surface of CDF nanomicelles. Finally, the attached gold nanoseeds were used to nucleate the growth of a gold nanoshell on the surface of the CDF nanomicelles. $NH_2OH \cdot HCl$ was used to reduce $HAuCl_4$ to bulk Au metal. The gold nanoshells on the outer surface can be heated by NIR lasers as photoabsorbers for NIR-triggered release of the contents, as well as for photothermal ablation therapy. The gold-shell-coated CDF nanomicelles (CDF-Au-shell nanomicelles) also showed a good response (less than 10 min) to a magnetic field (**Figure 1**a,b), suggesting that the magnetic CDF-Au-shell nanomicelles would have great potential in magnetic-targeting drug-delivery technology for the treatment of cancer.

UV–vis spectra of the CDF-Au-shell nanomicelles at different stages of preparation are shown in Figure 1c–g. The extinction spectrum of the blank CSS vesicles exhibited no obvious peak in the range from 400 nm to 900 nm (Figure 1c) as a result of light scattering of the nanoparticles.[16] The peak at around 480 nm observed in Figure 1d,e was attributed to the absorbance of DOX. This demonstrates the successful DOX loading into the CDF nanomicelles. After Au-seed adsorption, the plasmon resonance peak around 550 nm for gold nanoparticles was observed (Figure 1f) and densely distributed dark spots could

be seen on the surface of CDF nanomicelles (Figure 1h). The diameter of CDF-Au-seed nanomicelles was evaluated to be around 392.2 ± 4.7 nm by DLS measurements, because they tend to cluster after the adsorption of gold seeds. A new broad peak ranging from 650 nm to 900 nm was observed after reduction of the gold seeds by $NH_2OH \cdot HCl$ (Figure 1g), and the resulting nanoparticles showed rough edges and seemed to be much more dense and compact (Figure 1i). The hydrodynamic diameter for CDF-Au-shell nanomicelles was evaluated to be 301.9 ± 3.4 nm by DLS measurements (Supporting Information, Figure S2), consistent with the TEM image. The broad absorbance between 650 nm and 900 nm suggests that the CDF-Au-shell nanomicelles would be suitable for NIR light-triggered release of drugs and photothermal therapy.[17] In addition, the absorbance increased linearly on elevating the concentration of the CDF-Au-shell nanomicelles in Roswell Park Memorial Institute (RPMI)-1640 medium and there was no significant change of size for CDF-Au-shell nanomicelles dispersed in deionized water and fetal bovine serum (FBS)-containing medium, indicating the good stability of these nanoparticles in biological media (Supporting Information, Figure S3,S4).

2.2. In Vitro Magnetic-Resonance Imaging

To evaluate the T_2 enhancing capability, CDF-Au-shell nanomicelles with various iron concentrations were investigated by T_2-weighted MR imaging and compared with that of sodium citrate modified Fe_3O_4 nanoparticles with the same iron concentration. As shown in **Figure 2**, the signal intensity of the MR imaging decreased with the increase of the iron concentration for both samples (CDF-Au-shell nanomicelles and sodium citrate-modified Fe_3O_4 nanoparticles). Figure 2b indicates that the T_2 relaxation time decreases as the concentration of iron increases and the trend is fitted well by a linear line within the analyzed range of iron concentrations for both samples. The weighted transverse-relaxivity value (r_2) for the CDF-Au-shell nanomicelles was measured as 61.5 mM Fe^{-1} s^{-1}, which was much higher than that for the sodium citrate-modified Fe_3O_4 nanoparticles (8.8 mM Fe^{-1} s^{-1}). The increase in the transverse relaxivity is attributed to assembly of nanoparticles into clusters or aggregates in nanomicelles, which raises the cross-sectional area.[18,19]

2.3. Temperature Elevation Induced by NIR Laser Irradiation

Continuous exposure of aqueous suspensions of CDF-Au-shell nanomicelles to NIR light resulted in rapid elevation of their temperatures, which is an important feature of gold nanoshells used for selective treatment of solid tumors. At a laser output power of 2 W, no obvious temperature change was observed when deionized water was exposed to NIR light (**Figure 3**). In contrast, an aqueous dispersion of CDF-Au-shell nanomicelles at different concentrations (0.01 mg mL^{-1}, 0.05 mg mL^{-1}, 0.1 mg mL^{-1}, and 0.2 mg mL^{-1}) achieved temperature elevations of 8 °C, 12 °C, 18 °C, and 24 °C, respectively. This verifies the excellent photothermal efficiency of the CDF-Au-shell

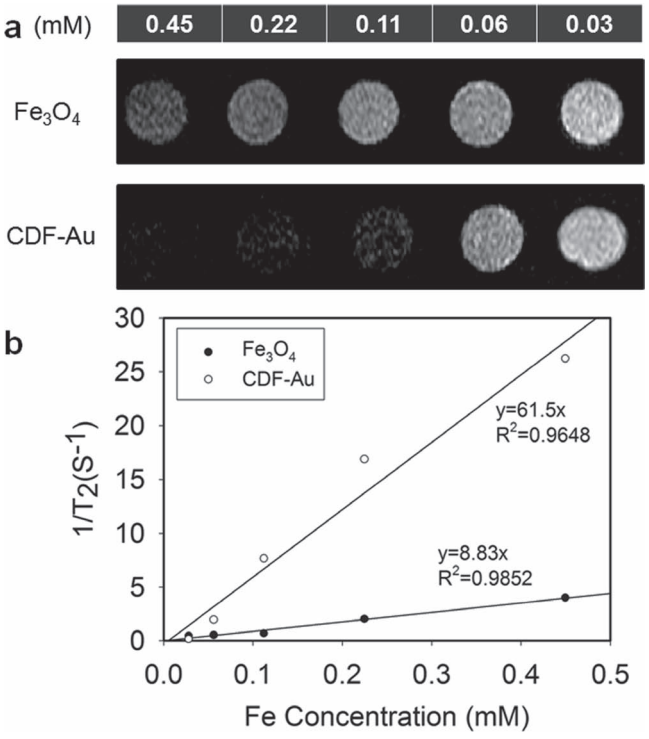

Figure 2. a) T_2-weighted MR imaging of CDF-Au-shell nanomicelles and Fe_3O_4 nanoparticles. b) T_2 relaxation rate ($1/T_2$) as a function of iron concentration (mM).

nanomicelles. At a concentration of 0.1 mg mL^{-1} or more, samples can be easily heated up to above 42 °C, which is sufficient to kill tumor cells.[20] These results suggest that the CDF-Au-shell nanomicelles could act as efficient NIR-light absorbers for photothermal tumor therapy.

2.4. Triggered Release of DOX by NIR Light

The CSS molecules showed a phase transition from gel to a liquid-crystalline state with a peak maximum (T_m) at 110.14 °C

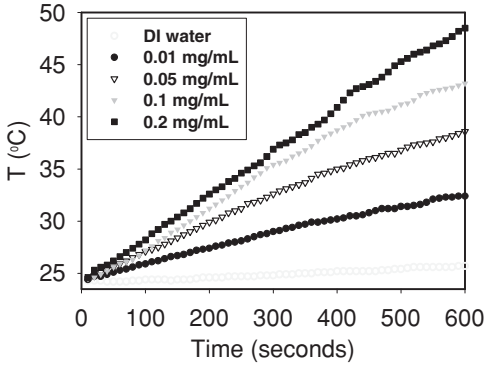

Figure 3. Temperature elevation in aqueous solutions containing CDF-Au-shell nanomicelles of different concentrations under NIR laser irradiation (808 nm, 2 W) measured every 10 s using a digital thermometer, over a period of 10 min.

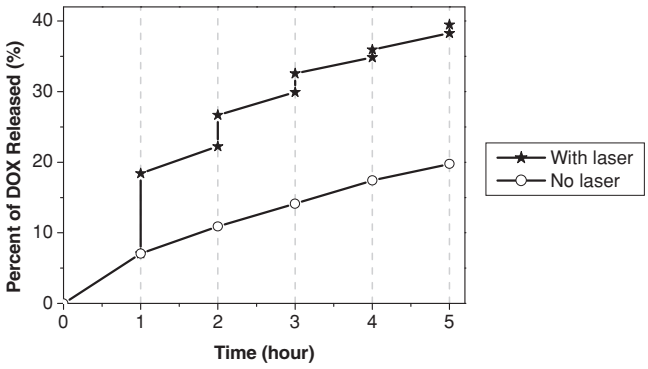

Figure 4. NIR-triggered release of DOX from CDF-Au-shell nanomicelles. The samples were irradiated with an NIR laser (2 W) for 10 min and the laser was turned off for the next 1 h. The control samples were not irradiated over the whole period.

(Supporting Information, Figure S5). The T_m value was high, although it is lower than that of cholesterol (150.4°C) due to the incorporation of (3-aminopropyl)triethoxysilane (APTES) into CSS molecules. The high T_m value could make CSS nanomicelles minimize the drug leakage during circulation and release the drug when needed, since the incorporation of gold nanoshells into CSS micelles to act as "NIR absorbers" allows for heating and resulting drug release by applying laser irradiation.

Figure 4 shows the characteristics of the DOX release from the CDF-Au-shell nanomicelles with or without irradiation by NIR light. The samples were irradiated repeatedly over a period of 10 min, followed by 1 h intervals with the laser turned off. A rapid release was observed upon NIR irradiation and the DOX release rate slowed down when the NIR irradiation was switched off. After the first NIR exposure for 10 min, the percentage of released DOX increased from 7.1% to 18.4%. The percentage increased to 19.7% over the whole period without NIR laser irradiation, significantly lower than that with NIR laser irradiation (39.5%). The gold nanoshell was formed by the reduction of $HAuCl_4$ on the surface of gold nanoseeds to nucleate the growth of a gold nanoshell on the surface of the CDF nanomicelles. Actually, it is the size growth process of these gold nanoseeds in situ, thus forming an incomplete shell on the surface of the nanomicelles, which is the reason for the drug release without laser irradiation. When the samples were exposed to NIR light five times for 10 min, the accumulated release amount of DOX over the whole experiment process was about two-fold greater than that without laser irradiation. Although the DOX release amount after each irradiation decreased from the first cycle to the fifth cycle, which would result from the increased coverage of gold nanoshells due to the melting effect of the gold nanostructures,[21] we successfully demonstrated a stepwise triggered release based on NIR exposure using the CDF-Au-shell nanomicelles. These multiple release kinetics can be attributed to the unique characteristics of the CSS nanomicelles. For traditional liposomes, they usually exhibit a one-time release profile instead of multiple release kinetics due to their instability and low T_m.[6] Most gold-nanoshell-coated liposomes would go through a melting and fusion process and are converted to large gold aggregates.[22] Compared with liposomes, CSS nanomicelles possess a much higher melting temperature, obviously reducing drug leakage. Moreover, the siloxane surface endows the CSS nanomicelles with a remarkably high mechanical stability and heat resistance. No obvious structure change is observed from the TEM image of the CDF-Au-shell nanomicelles after five cycles of irradiation (Supporting Information, Figure S6).

2.5. Photothermal Cytotoxicity of CDF-Au-Shell Nanomicelles

For qualitative analysis, staining of viable cells with calcein acetoxymethyl ester (calcein AM) and staining of dead cells with propidium iodide (PI) were performed to verify the photothermal effect of the CDF-Au-shell nanomicelles. After laser exposure of 8 W cm^{-2} for 10 min, a red-fluorescent region indicating dead cells was observed only in the presence of both the CDF-Au-shell nanomicelles and the laser irradiation (**Figure 5**, image j–l), indicating all of the cells within the laser spot underwent photothermal destruction. In comparison, other samples (Figure 5, image a–i) showed a vivid green color over the entire area, suggesting that the CDF-Au-shell nanomicelles alone or a NIR laser alone would not induce cell death. The dark region in image j in Figure 5, as well as the red region in image k in Figure 5 match the area where the NIR laser irradiation was performed, thus demonstrating that the CDF-Au-shell nanomicelles would cause cell death through photothermal effects only under NIR laser irradiation.

2.6. In Vitro Cell Viability

To investigate the combined effects of photothermal cytotoxicity, magnetic targeting and chemotherapy of CDF-Au-shell nanomicelles further, the cell viability of HeLa cells incubated with free or loaded DOX of different concentrations, with or without laser irradiation and a magnetic field was determined by 3-(4, 5-dimethylthiazol-2-yl)-2,5-diphenyltetrazolium bromide (MTT) assay. As shown in **Figure 6**a, cells treated with nanomicelles of various concentrations (0.05 μM, 0.5 μM, 5 μM) showed a relatively lower cell viability compared with the control group without laser irradiation, suggesting the effect of DOX acting as chemotherapeutic drug. The cell viability for the cells treated with CDF nanomicelles or CDF-Au-shell nanomicelles was not obviously changed after exerting the magnetic field (Figure 6b), which could have resulted from the short incubation time of the nanomicelles with the cells, and the lower amount of DOX released. When exposing the cells to CDF-Au-shell nanomicelles with the NIR laser alone, although not obvious, a decrease of cell viability (80% in Figure 6a vs 73% in Figure 6c) was observed at the concentration of 5 μM, which would due to the small amount of CDF-Au-shell nanomicelles internalized by the cells in the absence of the magnetic field (Supporting Information, Figure S7,S8). Noticeably, after incubation with 5 μM CDF-Au-shell nanomicelles, the cellular uptake amount of these nanoparticles into the Hela cells increased greatly under a magnetic field, as shown in the microscopic images and the iron-content measurements. Therefore, the cell viability

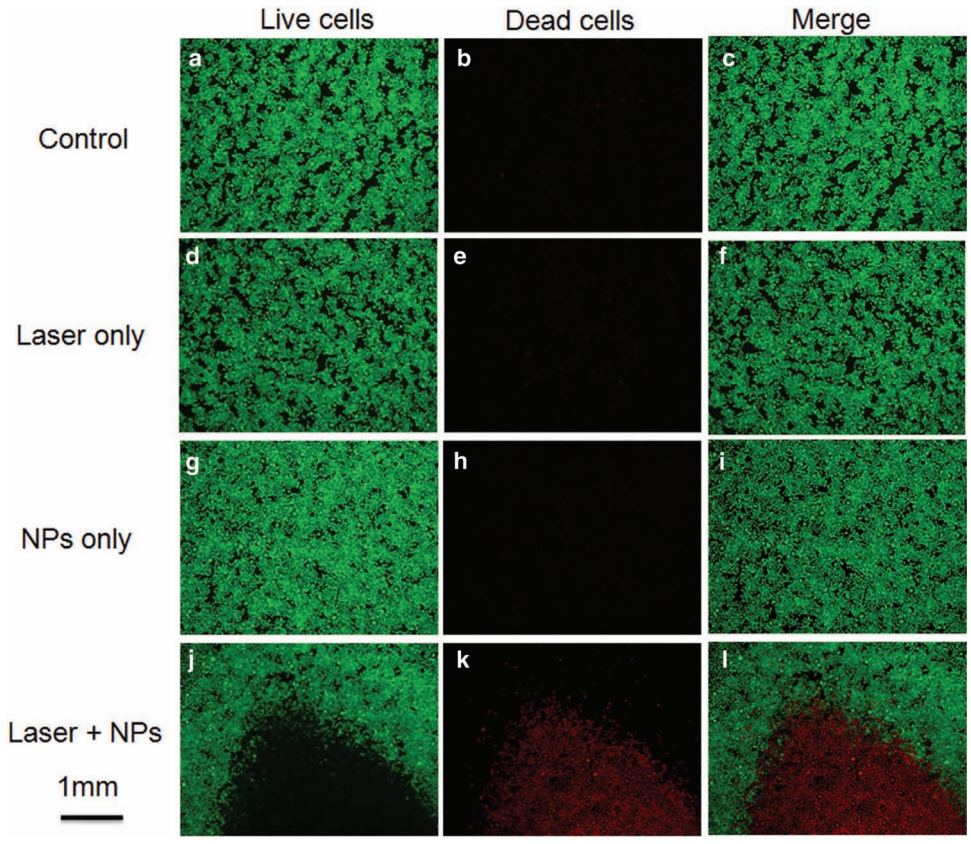

Figure 5. Fluorescence microscopy images of HeLa cells with different treatments, stained with calcein AM and PI. The green and red areas represent the regions of living and killed cells, respectively. (CDF-Au-shell nanomicelles concentration: 0.1 mg mL^{-1}; NIR laser: 808 nm, 8 W cm^{-2}, 10 min).

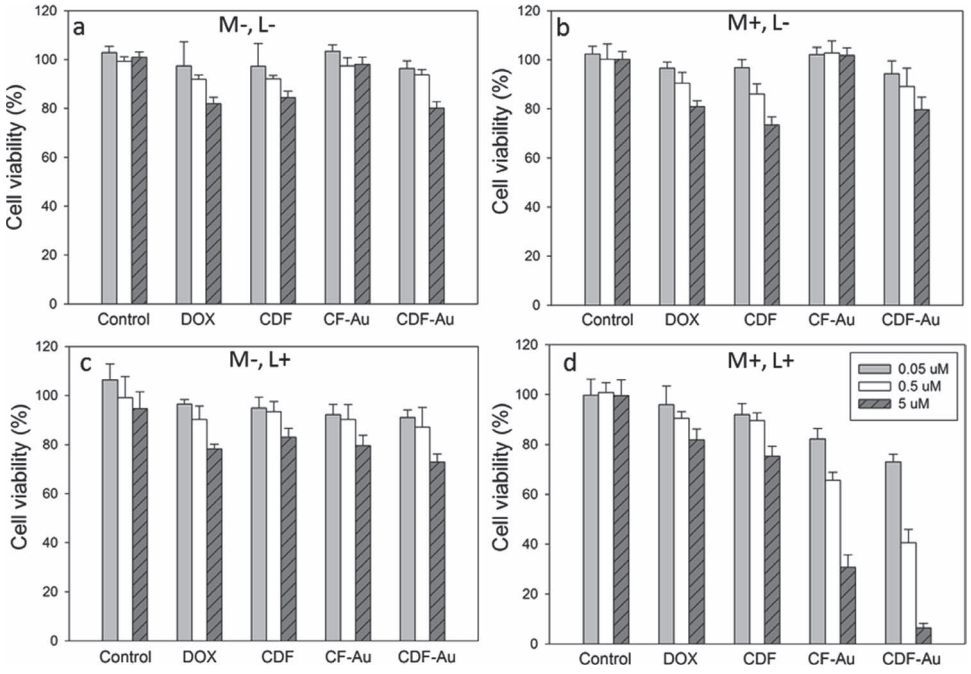

Figure 6. Cell viabilities after incubation with different dosages (0.05 μM, 0.5 μM, 5 μM) of DOX, CDF nanomicelles, and CDF-Au-shell nanomicelles, with or without a magnetic field and laser irradiation (808 nm, 4 W cm^{-2}, 10 min). The CF-Au and CDF-Au samples had the same iron concentrations. M and L represented the magnetic field and laser, respectively. The data are shown as mean ± standard deviation (SD), $n = 3$.

for the CDF-Au-shell nanomicelles was inhibited greatly (less than 10%) compared with those for the DOX-free CF-Au-shell nanomicelles (31%) when exerting both the NIR laser and the magnetic field (Figure 6d).

These results reveal that the combination of chemotherapy, magnetic targeting, and photothermal therapy through the CDF-Au-shell nanomicelles is expected to increase the likelihood of cell killing significantly, to improve the selectivity greatly and, potentially, to overcome resistance to chemotherapeutic agents, making it a promising approach for cancer therapy. CDF-Au-shell nanomicelles could be guided to the tumor area by a magnetic field, followed by NIR laser irradiation at the tumor site, which should enhance the targeting effectiveness. The permeability of tumor vessels and the sensitivity of the tumor cells toward chemotherapeutics should be greatly enhanced by hyperthemia, holding the promise of improving drug efficacy. In addition, photothermal therapy may facilitate triggered and instant drug release from the nanoparticles, which is critical for achieving a high effective drug concentration in the tumor. Moreover, one of the major advantages of NIR laser light as a source of hyperthermia is that the exposures are non-invasive and applied extracorporally, compared with other types of hyperthermia like radiofrequency ablation or microwave ablation, which require interstitial needle or antenna insertion.

3. Conclusions

In summary, we have synthesized CDF-Au-shell nanomicelles as a multifunctional platform to combine MR imaging, magnetic-targeted drug delivery, NIR light-triggered drug release, and photothermal therapy into one system simultaneously. The resulting CDF-Au-shell nanomicelles display enhanced T_2-weighted MR imaging and surface plasmon absorbance in the NIR region, thus exhibiting an NIR-induced temperature elevation and an NIR light-triggered and stepwise release behavior of doxorubicin. Photothermal cytotoxicity and cell-viability tests in vitro indicated the feasibility of using the CDF-Au-shell nanomicelles in photothermal treatment under NIR irradiation. Importantly, a synergistic effect in killing cancer cells was found by the combined photothermal therapy and the magnetic-field-guided drug delivery. The "all-in-one" drug-delivery system, which combines all of the functional units into one nanoparticle, has provided us with unprecedented opportunities for developing advanced, targeting drug-delivery system. Future studies employing more-advanced CSS nanomicelle systems for both spatially and temporally improved hyperthermia, magnetic-resonance contrast agents for in vivo monitoring of tissue pharmacokinetics, and hence more-efficient optimization of hyperthermia may lead to further refinements in targeting and delivery of drugs.

4. Experimental Section

Materials: Cholesteryl-succinyl silane (CSS) was synthesized according to the reported method.[12] Hydroxylamine hydrochloride ($NH_2OH{\cdot}HCl$) (1.5 mL, 40 mmol L^{-1}, Shanghai Shanpu Chemical, China) was used as received. Hydrogen tetra-chloroaurate (III) hydrate ($HAuCl_4{\cdot}4H_2O$), sodium citrate and sodium borohydride ($NaBH_4$) were obtained from SinoReagent, China. Doxorubicin hydrochloride (DOX•HCl) was obtained from Beijing Huafeng United Technology. MTT was purchased from Sigma. The other chemicals were purchased from the Beijing Chemical Company. Deionized water (18.2 MΩ·cm) from a Milli-Q Gradient System was used in all of the preparations. All of the chemicals were of analytical grade and used directly without further purification.

Synthesis of Magnetic Iron Oxide (Fe_3O_4) Nanoparticles: Oleic acid-stabilized Fe_3O_4 nanoparticles were synthesized by a coprecipitation method.[15] $FeCl_3{\cdot}6H_2O$ (13.6 g) and $FeSO_4{\cdot}7H_2O$ (13.9 g) were dissolved in deionized water (100 mL) contained in a four-neck flask, followed by addition of $NH_3{\cdot}H_2O$ solution (30 mL) with agitation at room temperature under a N_2 atmosphere. Then, the aqueous solution was heated to 80 °C for 30 min. To obtain the well-dispersed Fe_3O_4 nanoparticles, oleic acid was added with vigorous stirring for another 30 min. The precipitate was isolated by an Nd-Fe-B magnet and washed three times with deionized water and four times with acetone. Then, the collected magnetic nanoparticles were dispersed in hexane for use.

Preparation of DOX-loaded Magnetic Nanomicelles (CDF Nanomicelles): The hydrophobic base form of DOX was first prepared by adding 2.0 equivalents of triethylamine (TEA) to the DOX•HCl solution and stirring for 1 h. CDF nanomicelles were prepared through an injection method: Fe_3O_4 nanoparticles (0.1 mg) dispersed in hexane were mixed with CSS dissolved in ethanol (1 mg), followed by the addition of a solution of DOX in chloroform/methanol (2:1, v/v). The obtained suspension was then injected slowly into deionized water (1 mL) under water-bath sonication. The molar ratio of DOX to CSS molecules was 1:30. The untrapped DOX was removed by centrifuging at 1500 rpm for 10 min. The amount of entrapped DOX was determined by measuring the fluorescence intensity of the drug-loaded CSS micelles at 480 nm after dissolving in dimethyl sulfoxide (DMSO).

Preparation of Citrate-Stabilized Gold Seeds: Citrate-stabilized gold nanoparticles with an average diameter of about 2.6 nm were prepared according to the literature.[23] Briefly, $HAuCl_4$ aqueous solution (1.0 mL, 1% w/v) was added into deionized water (100 mL), followed by the addition of 1.0 mL of sodium citrate solution (1% w/v) with vigorous stirring. Then $NaBH_4$ (1.0 mL, 0.075% w/v) in sodium citrate (1% w/v) solution was added and continuously stirred for 5 min, and then stored at 4 °C before use.

Fabrication of the Gold-Nanoshell-Coated CDF (CDF-Au-Shell Nanomicelles): The CDF-Au-shell nanomicelles were fabricated by electrostatic deposition of gold nanoparticles onto the positive charged surface of the CDF nanomicelles, followed by surface seeding.[24] Gold seed solution (2 mL) was added into 1 mL of a CDF suspension in a 5 mL tube, shaken and mixed for about 5 min; then, Au-seed-coated (CDF-Au-seed) nanomicelles were obtained by magnetic separation after three washes. The CDF-Au-seed nanomicelles were resuspended in deionized water (0.5 mL) followed by the addition of $HAuCl_4$ (1.2 mL, 5.08 mM). Then, $NH_2OH{\cdot}HCl$ (100 µL, 2.78% w/v) was added dropwise and stirred for about 30 min to allow the reduction of $HAuCl_4$, forming nanoshells around the nanomicelle surface. For PEGylation, CDF-Au-shell nanomicelles (10 mg) were mixed with methoxy-poly(ethylene glycol)-thiol (mPEG-SH) (5 kD, Kaizheng Biotech., Beijing) (1 mg) and reacted for 24 h at room temperature. After reaction, the unreacted molecules were removed by repeated centrifugation.

Characterization of Nanomicelles: The UV–vis extinction spectra of the CSS vesicles, CDF, CDF-Au-seed, and CDF-gold-shell nanomicelles were analyzed using a UV–vis spectrophotometer (Varian Cary 4000) with a quartz cuvette of 1 cm optical path length to monitor the fabrication progress.

The morphology of the CDF, CDF-Au-seed, and CDF-Au-shell nanomicelles was observed using an FEI Quanta 200 scanning electron microscope. The suspensions of prepared nanomicelles were deposited onto a carbon-coated copper grid. After air-drying at room temperature, the nanomicelles were observed using a Hitachi H-7650 transmission electron microscope (TEM) equipped with a charge coupled device (CCD) camera. The accelerating voltage was 120 kV. The size

distributions of the CDF, CDF-Au-seed, and CDF-Au-shell nanomicelles were determined using a 90plus/BI-MAS DLS analyzer (Brookhaven Instruments Co., USA). The zeta potentials of the nanomicelles before and after the deposition of gold seed and the formation of the gold nanoshell were calculated from the electrophoretic mobility measured using a Brookhaven ZetaPALS instrument.

In Vitro Magnetic Resonance Imaging: All of the MR imaging experiments were performed using a 0.5 T NMR Analyzing & Imaging system (MiniMR-60, Shanghai Niumag Corporation) with a circularly polarized transmit-receive knee coil. The microscopic transverse relaxation time (T_2) was measured for various concentrations of CDF-Au-shell nanoparticles by applying spin-echo (SE) sequences at room temperature with T_R = 4000 ms and increasing the echo time (T_E) for successive scans: T_E = 60 ms. The other parameters were as follows: point resolution = 156 μm × 156 μm, section thickness = 0.6 mm, number of acquisitions = 1. After data collection, the regions of interest were drawn, and the mean signal intensity in each tube was recorded. The relaxivity value (r_2 in mM^{-1} s^{-1}) was calculated using T_2 measurements made with a series dilution of the CDF-Au-shell nanoparticle suspension in water. The iron concentration was determined by inductively coupled plasma-emission (ICP) spectrometry (Perkin Elmer, Optima 5300DV).

Temperature Elevation Induced by NIR Laser Irradiation: CDF-Au-shell nanomicelles of various concentrations were added to quartz cuvettes (total volume of 4.0 mL), irradiated with a continuous-wave diode NIR laser (T808D2W, Xi'an Minghui Optoelectronic Technology, China), with a center wavelength of 808 ± 10 nm and an output power of 2 W, for 10 min. The temperature of the solutions was measured using a digital thermometer with a thermocouple probe every 10 s.

Triggered Release of DOX by NIR Light: DOX release was performed in fresh phosphate buffered saline (PBS) (2.4 mL volume for each sample) for each time point. The sample suspensions were exposed to the same laser power of 2 W for 10 min (LASER ON) and then incubated at 25 °C for 1 h (LASER OFF). PBS from each time point was removed by magnetic separation and stored at 4 °C until analysis. The DOX release was determined by fluorescence-intensity readings (excitation at 480 nm; emission at 590 nm) using a Varian Cary Eclipse.

Photo-hyperthermic Effect on Cancer Cells: The photothermal cell toxicity of the CDF-Au-shell nanomicelles was evaluated on HeLa cells (human cervical carcinoma cell line). Cells (5×10^5 cells per well) were incubated overnight in 6-well plates at 37 °C in a humidified atmosphere containing 5% CO_2. After incubation with CDF-Au-shell nanomicelles (1.0 mL per well, 0.1 mg mL^{-1}) for 4 h, the cells were then exposed to an NIR laser (8 W cm^{-2}) for 10 min and stained with calcein AM and PI to verify the photo-hyperthermic effect on the cancer cells.

In Vitro Cell Viability: HeLa cells (1×10^4 cells per well) were seeded in 96-well plates and incubated overnight to allow the cells to attach to the surface of the wells. The cells were then exposed to 0.05, 0.5, and 5 μM of free DOX, CDF nanomicelles, and CDF-Au-shell nanomicelles with or without a magnetic field for 4 h. Afterwards, the supernatants were discarded, the cells were washed twice with PBS and irradiated by an NIR laser (4 W cm^{-2}) for 10 min. The cell viabilities were determined by MTT assay.

Statistical Analysis: The level of significance in all of the statistical analyses was set at a probability of $p < 0.05$. The ata are presented as the mean ± SD. Analysis of variance (ANOVA) and *t*-tests were used to analyze the data.

Supporting Information

Supporting Information is available from the Wiley Online Library or from the author.

Acknowledgements

This research was financially supported by the National Natural Science Foundation of China (NSFC-30970829) and the National Basic Research Program of China (973 Program, 2011CB707502).

Received: June 19, 2012
Revised: August 16, 2012
Published online: September 27, 2012

[1] H. Park, J. Yang, J. Lee, S. Haam, I. H. Choi, K. H. Yoo, *ACS Nano* **2009**, *3*, 2919.
[2] H. Y. Liu, D. Chen, L. L. Li, T. L. Liu, L. F. Tan, X. L. Wu, F. Q. Tang, *Angew. Chem. Int. Ed.* **2011**, *50*, 891.
[3] C. M. Cobley, J. Y. Chen, E. C. Cho, L. V. Wang, Y. N. Xia, *Chem. Soc. Rev.* **2011**, *40*, 44.
[4] D. Needham, G. Anyarambhatla, G. Kong, M. W. Dewhirst, *Cancer Res.* **2000**, *60*, 1197.
[5] E. Reimhult, E. A. Amstad, E. J. Kohlbrecher, E. Muller, T. Schweizer, M. Textor, *Nano Lett.* **2011**, *11*, 1664.
[6] X. H. Gao, Y. D. Jin, *J. Am. Chem. Soc.* **2009**, *131*, 17774.
[7] C. Alric, J. Taleb, G. Le Duc, C. Mandon, C. Billotey, A. Le Meur-Herland, T. Brochard, F. Vocanson, M. Janier, P. Perriat, S. Roux, O. Tillement, *J. Am. Chem. Soc.* **2008**, *130*, 5908.
[8] H. B. Na, I. C. Song, T. Hyeon, *Adv. Mater.* **2009**, *21*, 2133.
[9] J. M. Kinsella, A. Ivanisevic, *J. Am. Chem. Soc.* **2005**, *127*, 3276.
[10] H. S. Wi, K. Lee, H. K. Pak, *J. Phys.: Condens. Matter* **2008**, *20*, 494211.
[11] C. R. Dass, T. L. Walker, E. E. DeCruz, M. A. Burton, *Drug Delivery* **1997**, *4*, 151.
[12] Y. Ma, Z. F. Dai, Z. B. Zha, Y. G. Gao, X. L. Yue, *Biomaterials* **2011**, *32*, 9300.
[13] Z. F. Dai, W. J. Tian, X. L. Yue, Z. Z. Zheng, J. J. Qi, N. Tamai, J. Kikuchi, *Chem. Commun.* **2009**, 2032.
[14] T. K. Jain, J. Richey, M. Strand, D. L. Leslie-Pelecky, C. A. Flask, V. Labhasetwar, *Biomaterials* **2008**, *29*, 4012.
[15] S. Z. Li, Y. Ma, X. L. Yue, Z. Cao, Z. F. Dai, *New J. Chem.* **2009**, *33*, 2414.
[16] T. H. Ji, V. G. Lirtsman, Y. Avny, D. Davidov, *Adv. Mater.* **2001**, *13*, 1253.
[17] X. J. Ji, R. P. Shao, A. M. Elliott, R. J. Stafford, E. Esparza-Coss, J. A. Bankson, G. Liang, Z. P. Luo, K. Park, J. T. Markert, C. Li, *J. Phys. Chem. C* **2007**, *111*, 6245.
[18] J. M. Kinsella, S. Ananda, J. S. Andrew, J. F. Grondek, M. P. Chien, M. Scadeng, N. C. Gianneschi, E. Ruoslahti, M. J. Sailor, *Adv. Mater.* **2011**, *23*, H248.
[19] L. L. Ma, M. D. Feldman, J. M. Tam, A. S. Paranjape, K. K. Cheruku, T. A. Larson, J. O. Tam, D. R. Ingram, V. Paramita, J. W. Villard, J. T. Jenkins, T. Wang, G. D. Clarke, R. Asmis, K. Sokolov, B. Chandrasekar, T. E. Milner, K. P. Johnston, *ACS Nano* **2009**, *3*, 2686.
[20] M. Paiva, D. J. Castro, M. Bublik, J. Sercarz, *J. Invest. Med.* **2006**, *54*, S381.
[21] C. X. Guo, J. L. Wang, Z. F. Dai, *Microchim. Acta* **2011**, *173*, 375.
[22] G. H. Wu, A. Mikhailovsky, H. A. Khant, J. A. Zasadzinski, *Methods Enzymol.* **2009**, *464*, 279.
[23] K. C. Grabar, K. J. Allison, B. E. Baker, R. M. Bright, K. R. Brown, R. G. Freeman, A. P. Fox, C. D. Keating, M. D. Musick, M. J. Natan, *Langmuir* **1996**, *12*, 2353.
[24] H. T. Ke, J. R. Wang, Z. F. Dai, Y. S. Jin, E. Z. Qu, Z. W. Xing, C. X. Guo, X. L. Yue, J. B. Liu, *Angew. Chem. Int. Ed.* **2011**, *50*, 3017.